Anodic Formation and Characterization of Nanoporous InP in Aqueous KOH Electrolytes

C. O'Dwyer,[a,b,c] D. N. Buckley,[a,b,]* D. Sutton,[b,d] and S. B. Newcomb[b,e]

[a]*Department of Physics, University of Limerick, Limerick, Ireland*
[b]*Materials and Surface Science Institute, University of Limerick, Limerick, Ireland*

The anodic behavior of highly doped ($>10^{18}$ cm^{-3}) n-InP in aqueous KOH was investigated. Electrodes anodized in the absence of light in 2–5 mol dm^{-3} KOH at a constant potential of 0.5–0.75 V (SCE), or subjected to linear potential sweeps to potentials in this range, were shown to exhibit the formation of a nanoporous subsurface region. Both linear sweep voltammograms and current-time curves at constant potential showed a characteristic anodic peak, corresponding to formation of the nanoporous region. No porous region was formed during anodization in 1 mol dm^{-3} KOH. The nanoporous region was examined using transmission electron microscopy and found to have a thickness of some 1–3 μm depending on the anodization conditions and to be located beneath a thin (typically ~40 nm), dense, near-surface layer. The pores varied in width from 25 to 75 nm and both the pore width and porous region thickness were found to decrease with increasing KOH concentration. The porosity was approximately 35%. The porous layer structure is shown to form by the localized penetration of surface pits into the InP, and the dense, near-surface layer is consistent with the effect of electron depletion at the surface of the semiconductor.
© 2006 The Electrochemical Society. [DOI: 10.1149/1.2354441] All rights reserved.

There is considerable interest in the electrochemical formation of porosity in semiconductors, from the perspective of both furthering the understanding of the phenomenon and developing potential applications.[1-8] Much of the work performed to date has focused on n-type and p-type silicon, although investigations of the formation of porous structures in III-V semiconductors such as GaAs[8-12] and InP[13-16] have also been reported. Controlled modulation of the pore diameter and pore growth direction in such semiconductors has been suggested as a method by which photonic crystals with a photonic bandgap in the near-infrared or visible region can be formed.[14,15] It has been shown that pore growth in semiconductors is affected by electrolyte concentration[13,17,18] as well as substrate type,[19] orientation,[20] and doping density.[21] Considerable progress has been made in understanding the basic mechanisms of pore formation in silicon under electrochemical conditions, and several pore formation models have been proposed to account for the range of observed pore types.[22-25] By comparison, only a limited number of investigations of the mechanism of pore formation in III-V semiconductors have been reported.[9-16]

Since holes in the valence band are required for anodic oxidation, n-type electrodes do not etch in the dark under "normal" depletion conditions. At highly positive potentials, however, tunneling of carriers across the depletion layer can occur and the resulting holes in the valence band enable etching to take place.[26] Since tunneling is sensitive to the surface condition of the semiconductor, the etching process that can take place under anodic bias may be strongly affected by crystallographic defects and surface impurities.[27] Consequently, anodic etching of n-type semiconductors is often localized, thereby giving rise to the formation of porous sub-surface microstructures.

This paper describes an investigation of the anodic formation of nanoporous InP in KOH electrolytes with concentrations in the range 2–5 mol dm^{-3}. The anodic processes were studied electroanalytically using potential sweep and constant potential techniques under a variety of conditions, and the resulting porous structures were characterized using transmission electron microscopy (TEM).

* Electrochemical Society Fellow.
[c] Present address: Tyndall National Institute, University College Cork, Cork, Ireland.
[d] Present address: Department of Applied Science, Limerick Institute of Technology, Limerick, Ireland.
[e] Present address: Glebe Scientific Ltd., Glebe Laboratories, Newport, County Tipperary, Ireland.
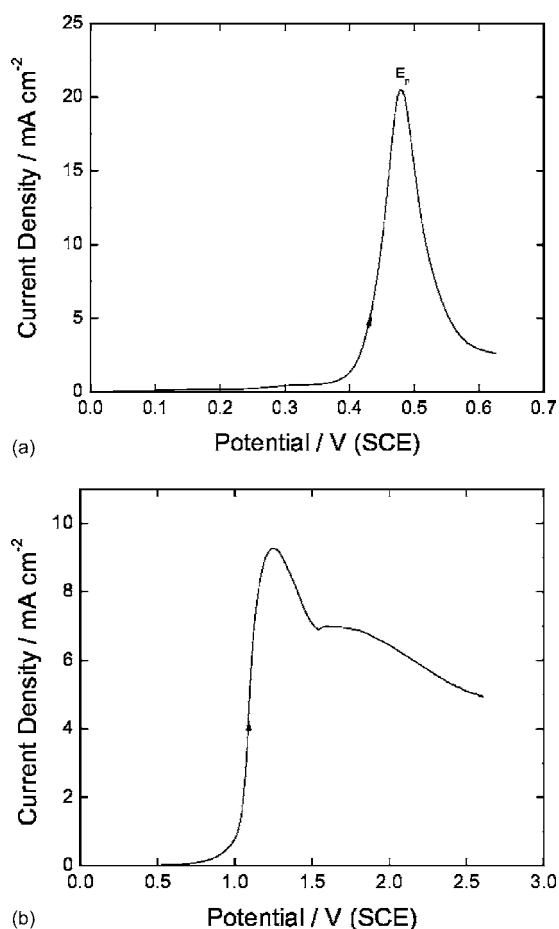
Experimental

The working electrode consisted of polished (100)-oriented sulfur-doped n-type indium phosphide (n-InP) grown by the liquid-encapsulated Czochralski (LEC) method and supplied by Sumitomo Electric, unless otherwise stated. As-received polished wafers had an essentially featureless surface when viewed at a magnification of 1000× under an optical microscope with Nomarski interference contrast (i.e., a typical surface finish for substrates for epitaxial growth). The nominal density of surface defects of the LEC wafers, as characterized by the etch-pit density (EPD), was in the 10^3 cm^{-2} range or lower. Wafers were cleaved into coupons (typically ~5 mm square) along the natural (110) cleavage planes and an ohmic contact was made by alloying indium to the back of the coupons. The back and the cleaved edges were electrically isolated from the electrolyte by means of a suitable varnish. The electrode area was typically 0.2 cm^2.

Anodization was carried out in aqueous KOH electrolytes with concentrations in the range 1–5 mol dm^{-3}. A conventional three-electrode cell configuration was used, employing a platinum counter electrode and a saturated calomel electrode (SCE) to which all potentials are referenced. Prior to immersion in the electrolyte, the working electrode was immersed in an etchant (3:1:1 H$_2$SO$_4$:H$_2$O$_2$:H$_2$O) for 4 min and then rinsed in deionized water. "Standard" n-InP working electrodes had a carrier concentration of ~3 × 10^{18} cm^{-3}. In experiments on the effect of carrier concentration, electrodes with lower (~5 × 10^{17} cm^{-3}, supplied by Lucent Technologies, grown by the vertical gradient freeze method) and higher (~6 × 10^{18} cm^{-3}) values were used where indicated in the text. All of the electrochemical experiments were carried out at room temperature and in the absence of light.

A CH Instruments model 650A Electrochemical Workstation interfaced to a Personal Computer (PC) was employed for cell parameter control and for data acquisition. The surfaces of the anodized samples were examined using a Veeco Explorer atomic force microscope (AFM). Electron transparent sections for plan-view and cross-sectional TEM examination were prepared by thinning to electron transparency using standard focused ion beam (FIB) milling procedures[28] in a FEI 200 FIB workstation. The TEM characterization was performed using a JEOL 2000FX TEM operating at 200 kV.

Results and Discussion

Electrochemical growth of nanoporous InP.— Figure 1a shows a linear sweep voltammogram (LSV) of an n-InP electrode in 5 mol dm^{-3} KOH. The potential was scanned at 2.5 mV s^{-1} from an initial potential of 0 V. There is little current at potentials less than

(a)

(b)

Figure 1. LSV at 2.5 mV s^{-1} of an n-InP electrode in (a) 5 mol dm^{-3} KOH and (b) 1 mol dm^{-3} KOH.

(a)

(b)

Figure 2. (a) Under-focus bright-field TEM micrograph of an n-InP electrode after an LPS from 0 to 0.63 V (SCE) at 2.5 mV s^{-1} in 5 mol dm^{-3} KOH. A nanoporous InP layer (A) is observed above the InP substrate (B) and beneath a dense near-surface layer (C). (b) Bright field TEM micrograph of an n-InP electrode cross section after a LPS from 0 to 1.3 V (SCE) at 2.5 mV s^{-1} in 1 mol dm^{-3} KOH. A thin surface film (A) is observed above the InP substrate (B). The surface of the sample was capped by the amorphous deposit marked at C during specimen preparation for TEM.

0.3 V, but continued anodization to potentials greater than 0.4 V results in a rapid increase in the current density to a peak value of 20 mA cm^{-2} at 0.48 V. Above 0.48 V, the current density decreases quite rapidly, reaching a value of ∼3 mA cm^{-2} at 0.6 V. A significant anodic process clearly occurs above ∼0.4 V and becomes self-limiting at higher potentials. Figure 1b shows a LSV of a similar n-InP electrode in 1 mol dm^{-3} KOH at the same scan rate (2.5 mV s^{-1}). As in Fig. 1a, an anodic peak can similarly be observed, but at a higher potential (∼1.25 V).

The electrodes formed during anodization in the two KOH electrolyte concentrations were examined using TEM. The micrographs shown in Fig. 2 demonstrate that the anodic processes are remarkably different in the two different concentrations of KOH. Figure 2a shows that anodization in 5 mol dm^{-3} KOH results in the formation of a nanoporous InP layer, and, as discussed later, similar nanoporous layers were observed in 2 and 3 mol dm^{-3} KOH. Figure 2a was taken in an under-focus condition and thereby uses phase contrast effects to enhance the visibility of the pores formed within the upper part of the InP. The sense of the Fresnel contrast changes seen as a function of the defocus conditions in through focal series of bright-field micrographs confirmed the formation of the low-density regions described, although it should be emphasized that the nanopores are heavily interspersed with a high volume fraction of microcrystalline material. Figure 2b, by comparison, shows that, after a similar linear potential sweep (LPS), there appears to be little change in the electrode during anodization in 1 mol dm^{-3} KOH other than a thin (∼25 nm) surface film, as marked at A. The results presented in this paper are for nanoporous InP formation in 2–5 mol dm^{-3} KOH. Preliminary results on the anodization of n-InP in
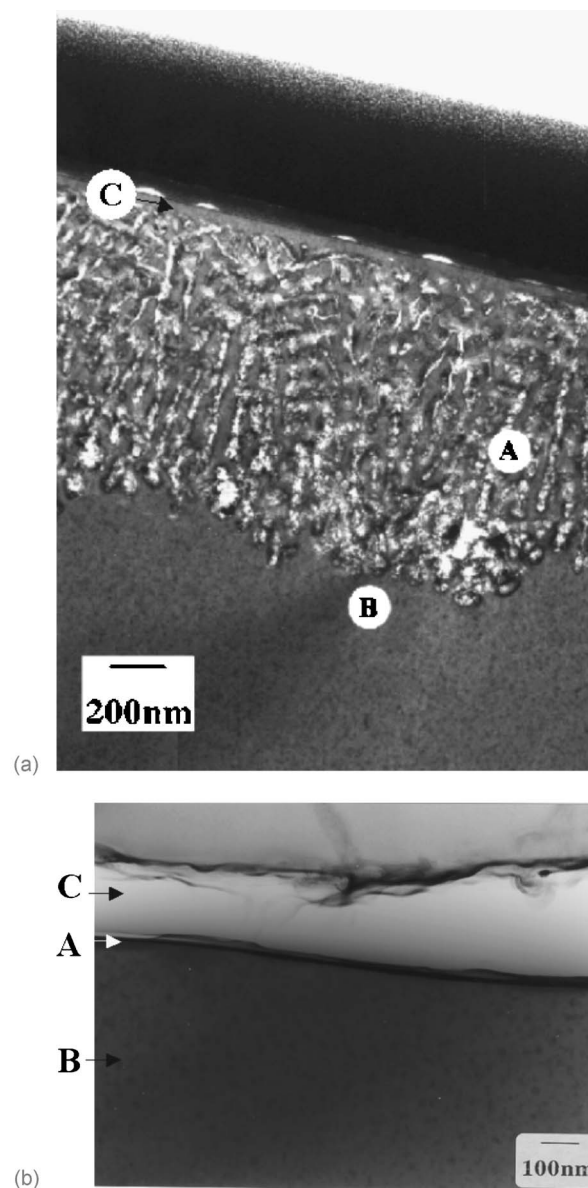
1 mol dm^{-3} KOH have been reported[29] and a detailed study will be described elsewhere. The transition to porous layer formation in electrolytes with concentrations in the range 1–2 mol dm^{-3} is currently being investigated.

LSVs were performed in 5 mol dm^{-3} KOH over a range of scan rates and in all cases an anodic current peak was observed,[30] as in Fig. 1a. While the current densities increase at higher scan rates, the charge density corresponding to the anodic peak was found to remain relatively constant (0.57 C cm^{-2}), indicating that an approximately equal amount of InP is oxidized irrespective of the scan rate.

TEM was used to examine the anodization process in further detail. Figure 2a shows the porous region, marked at A, extending ∼1 μm into the InP substrate (B), and capped by a thin layer (∼40 nm) close to the surface that appears to be unmodified (C).
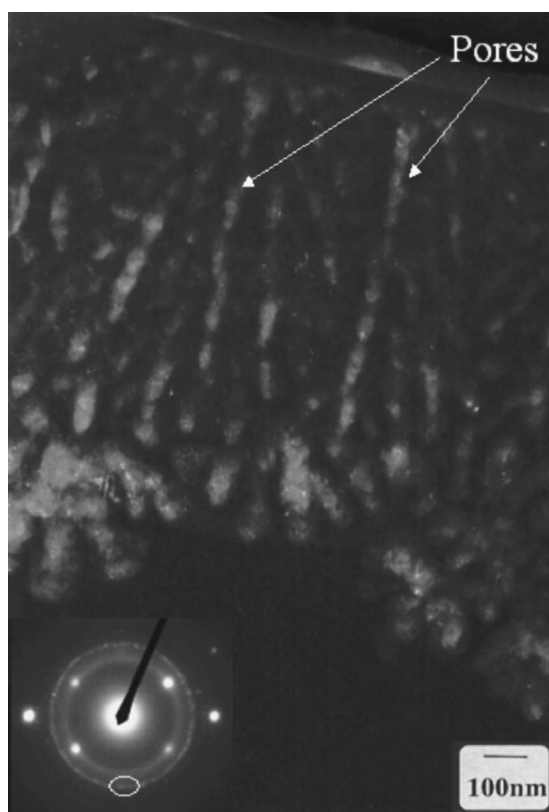
Figure 3. Dark-field TEM micrograph of the region marked at A in Fig. 2 and associated electron-diffraction pattern.

The thickness of the nanoporous region is generally uniform, although in some cross sections the interface with the substrate was characteristically found to be nonplanar. The average pore width and interpore distances are noted to be similar (~ 40 nm) to one another as well as to the thickness of the near-surface layer. Figure 3 shows a higher magnification dark-field TEM micrograph of part of the region shown in Fig. 2a and from where the inset diffraction pattern was taken. The pattern itself demonstrates the unmodified form of the nonporous parts of the InP electrode given the near [110] orientation of the InP.

The mechanism by which a porous region can form within the substrate by electrochemical oxidation despite the presence of this dense InP layer at the surface at first sight appears to be inconsistent with the microstructures seen in Fig. 2 and 3. The near-surface region of the anodized InP, however, was found to contain a sparse distribution of localized channels, and one such area is shown in dark field in Fig. 4. The dense, near-surface layer can be seen to contain a channel (at A) from which the pores underlying it appear to emanate. This observation suggests a mechanism by which the porous layer can grow, i.e., the porous region is connected to the bulk electrolyte via localized channels within the near-surface layer. Further evidence for the existence of these channels was obtained from AFM examination of the surface of electrodes after anodization, as discussed in detail elsewhere.[31] It is assumed that both the porous layer and the channels through the near-surface layer are filled with electrolyte, which connects the porous structure with the bulk electrolyte. This enables ionic current to flow and electrochemical oxidation of InP to proceed, thus providing a mechanism by which the porous layer can grow. The channels contained within the near-surface layer can thus be seen to play a critical role in the formation of the nanoporous structure.

Effect of electrolyte concentration.— Experiments were carried out at lower KOH concentrations. Figure 5 shows LSVs of InP
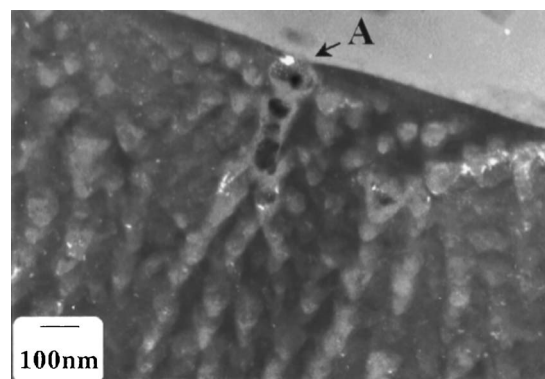

Figure 4. Dark-field TEM cross-sectional micrograph of the near-surface region of an InP electrode after an LPS from 0 to 0.63 V (SCE) at 2.5 mV s^{-1} in 5 mol dm^{-3} KOH. A channel has been formed through the near-surface layer of the electrode (at A).

electrodes in 2 and 3 mol dm^{-3} KOH under similar conditions to those given in Fig. 1. A similar overall response is seen in Fig. 5 as in 5 mol dm^{-3} KOH: anodic current peaks are observed at 0.46 V in 3 mol dm^{-3} KOH and at 0.52 V in 2 mol dm^{-3} KOH. A shoulder is also observed on the higher potential side of the peak in the 3 mol dm^{-3} curve and a second peak at 0.7 V in the 2 mol dm^{-3} curve.

Cross-sectional TEM demonstrated the formation of nanoporous layers corresponding to the observed anodic currents in these electrolytes. Figure 6a and b shows bright-field images of electrodes that had been subjected to potential sweeps from 0 to 0.825 V in 2 mol dm^{-3} KOH and from 0 to 0.675 V in 3 mol dm^{-3} KOH, respectively. In each case, a porous zone similar to that described above for the 5 mol dm^{-3} KOH was found to have been formed, and the porous region is capped by a thin, dense, near-surface layer. The ~ 40 nm near-surface layer was again found to contain a number of channels, as at A in Fig. 6b.

Experiments at constant potential in 2–5 mol dm^{-3} KOH.— Experiments were carried out at constant potential. A series of experiments was performed in 5 mol dm^{-3} KOH, in which the potential was stepped from open circuit to potentials in the range 0.5–0.75 V (i.e., where nanoporous layer formation is observed on a typical LSV). Figure 7 shows the current-time curves obtained at potentials of 0.5, 0.6, and 0.75 V. In each case, the current initially
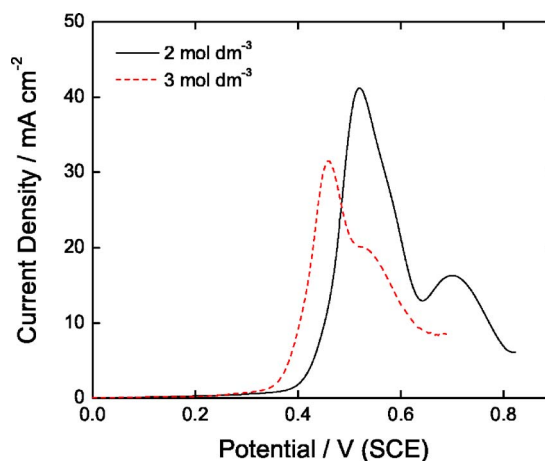

Figure 5. (Color online) LSVs of InP electrodes at 2.5 mV s^{-1} from an initial potential of 0 V (SCE) in (a) 2 mol dm^{-3} KOH and (b) 3 mol dm^{-3} KOH.
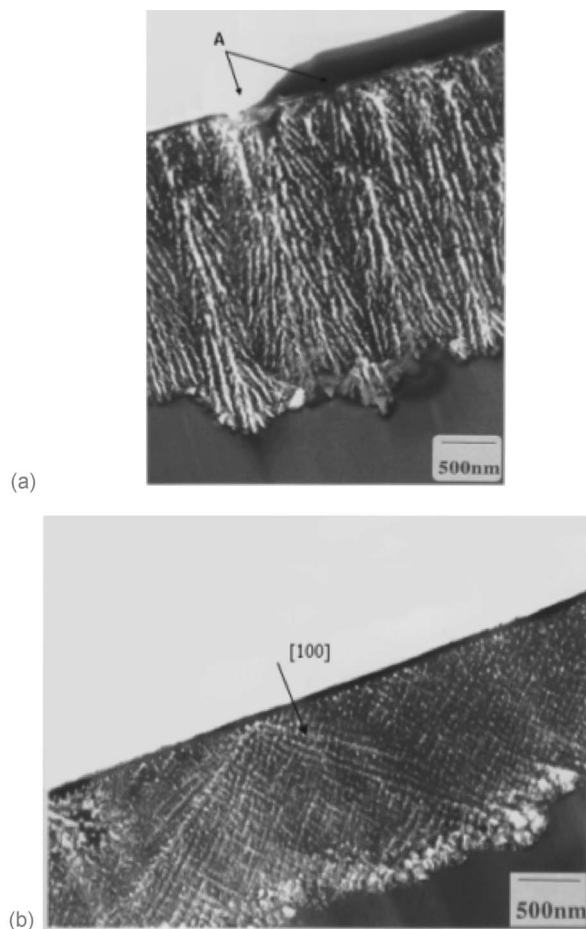
Figure 6. Cross-sectional bright-field TEM micrograph of an InP electrode after a LPS (a) in 2 mol dm^{-3} KOH from 0 to 0.825 V (SCE) and (b) in 3 mol dm^{-3} KOH from 0 to 0.675 V (SCE). The scan rate was 2.5 mV s^{-1}.

increases with time, reaching a peak after 23 s (0.5 V), 8 s (0.6 V), and 5 s (0.75 V), and subsequently decreases. The peak current density can be seen to rise and shift to shorter time with increasing potential.

Cross-sectional TEM examination was performed on electrodes anodized for 100 s at 0.5, 0.6, and 0.75 V (see Fig. 7). Figure 8a-c shows bright-field images of typical near-surface regions of the elec-
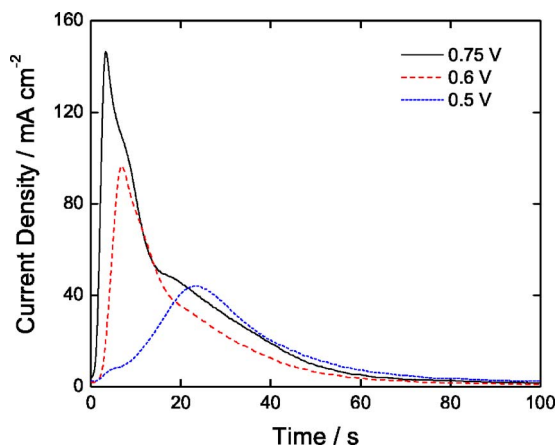

Figure 7. (Color online) Current-time curves for InP electrodes in 5 mol dm^{-3} KOH at potentials of (a) 0.5 V, (b) 0.6 V, and (c) 0.75 V (SCE).

trodes formed at the three potentials. In each case, a nanoporous region has been formed beneath a thin near-surface layer, as was observed under potential sweep conditions. The near-surface layer was shown by electron diffraction to be essentially unmodified InP and thus to be in the same orientation as that of the bulk substrate. The pore size as well as the pore morphology vary somewhat as a function of potential. Similar observations have been reported for InP electrodes anodized galvanostatically in HCl-based electrolytes.[15,32] Channels within the near-surface layer were again found to have been formed and an example can be seen at G in Fig. 8a. Figure 9 is a higher magnification dark-field image of a sample that was anodized at 1.1 V for 100 s and provides further evidence for channels that extend through the full thickness of the near-surface layer, as at A and B.

Constant potential experiments were also carried out at lower KOH concentrations. Typical current-time curves of InP electrodes at 0.75 V in 2 mol dm^{-3} KOH and 3 mol dm^{-3} KOH as well as in 5 mol dm^{-3} KOH are shown in Fig. 10. Cross-sectional TEM was used to confirm the formation of nanoporous layers corresponding to the observed anodic currents in these electrolytes, Fig. 11a and b showing the near-surface regions of electrodes that had been subjected to anodization at a constant potential of 0.75 V for 150 s in 2 and 3 mol dm^{-3} KOH, respectively. In each case, a nanoporous layer similar to that obtained in 5 mol dm^{-3} KOH has been formed and is capped by a thin, dense, near-surface layer.

Characteristics of the nanoporous region.— The average values of thickness of the nanoporous layers formed under potential sweep conditions in 2, 3, and 5 mol dm^{-3} KOH were determined from TEM micrographs such as those shown in Fig. 2a and 6. The mean pore width was also estimated from higher-magnification micrographs of each porous layer. The dependence of the porous layer thickness and mean pore width on the electrolyte concentration is shown in Fig. 12, in which the porous layer thickness as well as the mean pore width can be seen to decrease with increasing KOH concentration. Measurements of porous layer thickness and mean pore width were similarly obtained from TEM micrographs of samples that had been potentiostatically anodized at 0.75 V in 2, 3, and 5 mol dm^{-3} KOH. Figure 13 shows the variation of the mean pore width and porous layer thickness with KOH concentration. It is observed that an increase in KOH concentration results in a decrease in both the pore width and the porous layer thickness, in a similar manner to that observed in Fig. 12. A similar trend has also been reported for porous silicon formed in HF solutions,[33] although lightly doped substrates have been found to show no changes in their mean pore width, or, in some instances, an increase with increasing electrolyte concentration at low current densities.

For each of the samples used in the layer thickness measurements described above, the corresponding charge density was estimated by integration of the current density with respect to time. The measured thickness of the porous layer was then plotted against the corresponding charge density, as indicated in Fig. 14. A theoretical value for the ratio of layer thickness to charge density was also estimated: using Faraday's law, the ratio of the thickness d of InP oxidized to the charge density Q is given by

$$\frac{d}{Q} = \frac{V_{M,InP}}{nF} \qquad [1]$$

where $V_{M,InP}$ is the molar volume of InP, n is the number of electrons per formula unit of InP, and F is the Faraday constant. Using a value[34] of 30.31 cm^3 mol^{-1} for $V_{M,InP}$ and assuming $n = 8$, a theoretical value of 0.393 μm C^{-1} cm^2 is estimated from Eq. 1 for d/Q, the ratio of layer thickness to charge density for complete removal of InP. This theoretical ratio is represented by the broken line in Fig. 14. The slope of the least-squares best fit line for the experimental data provides an estimate of 1.13 μm C^{-1} cm^2 for the corresponding ratio d_e/Q of experimental porous layer thickness d_e to charge density. The ratio of these estimates of d/Q and d_e/Q gives a value of $r = d/d_e = 0.347$, i.e., the estimated thickness of a compact InP
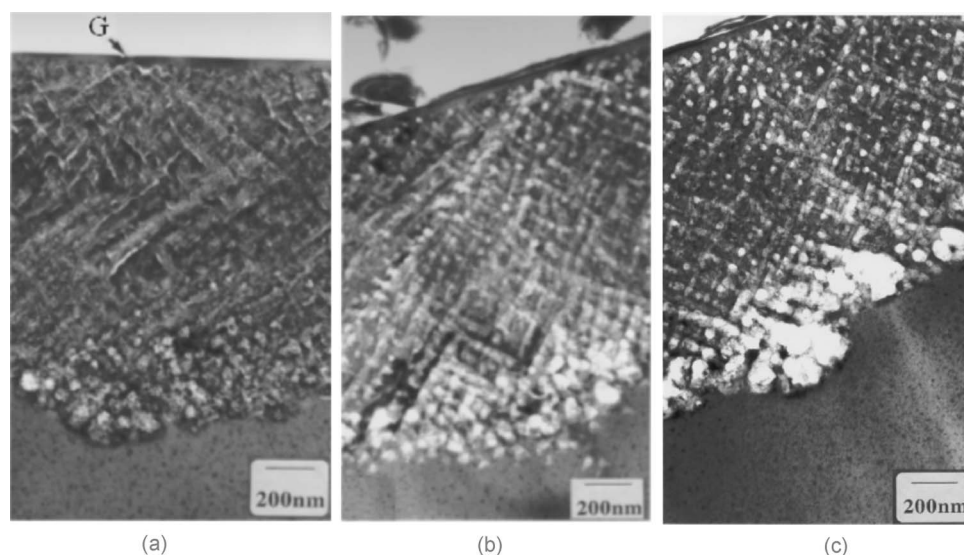
Figure 8. Cross-sectional bright-field TEM micrographs of InP electrodes after constant potential anodization at (a) 0.5 V, (b) 0.6 V, and (c) 0.75 V (SCE) for 100 s in 5 mol dm^{-3} KOH.

layer, which represents the quantity of InP removed, is a fraction $r = 0.347$ of the corresponding as-measured porous layer thickness. The porosity of the layers formed after anodization of InP in KOH electrolytes is thus estimated to be ~35%.

Effect of carrier concentration.— Experiments were carried out on wafers with lower (~5×10^{17} cm^{-3}) and higher (~6×10^{18} cm^{-3}) carrier concentrations than that of the standard (~3×10^{18} cm^{-3}) n-InP used in the anodization treatments described above. Each substrate was subjected to an LPS at 2.5 mV s^{-1} from an initial potential of 0 V, and the resulting LSVs are shown in Fig. 15. By comparison with the standard n-InP, it is clear that the higher doped n-InP electrode gives a similar current peak but at a considerably lower potential. The peak current density (24 mA cm^{-2}) is slightly higher than for the standard InP (20 mA cm^{-2}) as is the corresponding charge density: 0.86 C cm^{-2} for the higher-doped InP as compared with 0.57 C cm^{-2} for the standard InP. A very much smaller anodic peak is obtained (peak current density of ~0.1 mA cm^{-2} and charge density of 0.012 C cm^{-2}), however, for the lower doped InP at a potential of 0.64 V.

Cross-sectional TEM examination of each of the electrodes was carried out after anodization. Figure 16 is a bright-field TEM image of the higher-doped InP electrode after a potential sweep from 0 to 0.3 V. A nanoporous region can be seen to have been formed beneath a thin near-surface layer, as was observed for the standard InP electrodes described above. The morphology of the porous region appears to be generally similar to that obtained for the standard InP electrode (Fig. 2a) after potential sweep anodization, although the thickness of the near-surface layer is now ~25 nm compared with ~40 nm for the standard InP. The mean pore width and the inter-pore distance seen in Fig. 16a are similarly rather lower (~25 nm) than for the standard InP (~40 nm). The thickness of the porous region of the higher-doped InP, as determined from lower magnification micrographs of the entire layer, is ~1.6 μm, in comparison with ~1 μm in the case of standard InP (Fig. 2a).

In sharp contrast with higher-doped InP and standard InP, cross-sectional TEM has demonstrated that no porous region is formed for the lower-doped InP electrode, and such an image is shown in Fig. 16b. This is consistent with the observation of a very small anodic current peak in Fig. 15 (~200 times lower than that measured for standard InP samples under similar conditions) and a correspondingly lower charge density.
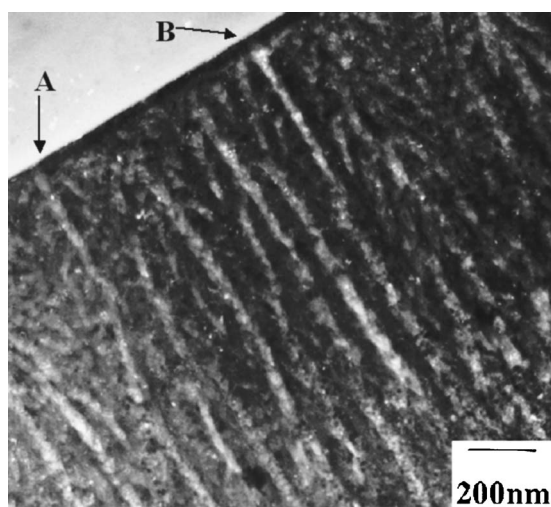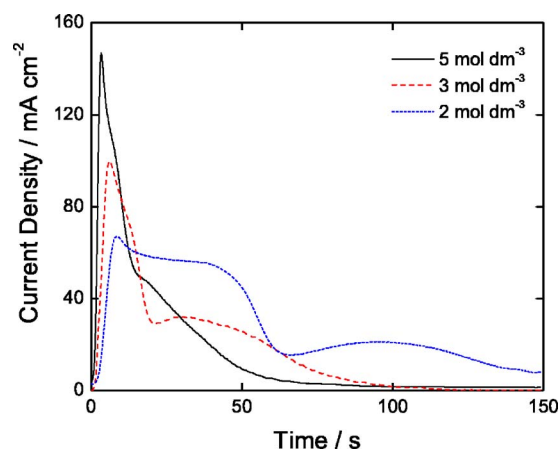

Figure 9. Cross-sectional dark-field TEM micrograph of an InP electrode after constant-potential anodization at 1.1 V (SCE) in 5 mol dm^{-3} KOH. Evidence for channels in the near-surface layer is shown at A and B.

Figure 10. (Color online) Current-time curves for InP anodized in (a) 2 mol dm^{-3}, (b) 3 mol dm^{-3}, and (c) 5 mol dm^{-3} KOH at a constant potential of 0.75 V (SCE).
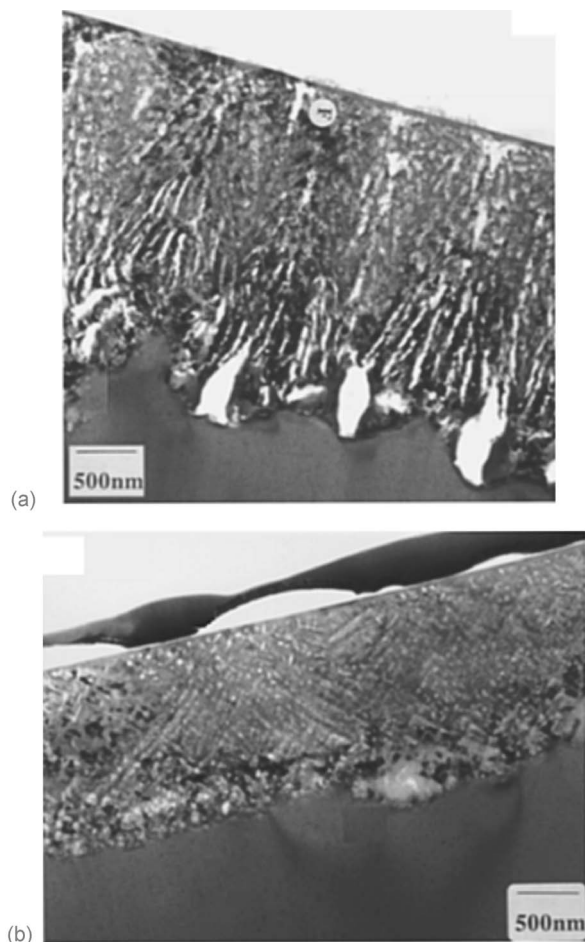
(a)

(b)

Figure 11. Cross-sectional bright-field TEM micrographs of n-InP electrodes after anodization at a constant potential of 0.75 V (SCE) in (a) 2 mol dm^{-3} KOH and (b) 3 mol dm^{-3} KOH for 150 s.

Pore growth process.— In the absence of light, n-InP can etch anodically only if holes are supplied by a breakdown mechanism, such as tunneling. The flatband potential measured[30] for a typical (n-type, $\sim 3 \times 10^{18}$ cm^{-3}) InP electrode in 5 mol dm^{-3} KOH was -1.45 V (SCE). Using an abrupt one-sided junction approximation,[26] this gives a value of 30 nm for the depletion layer
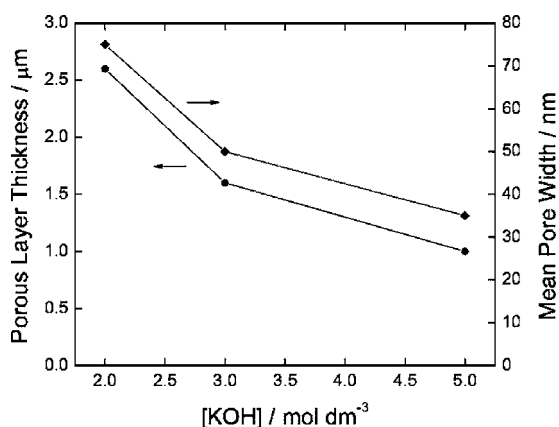

Figure 12. Plots of porous-layer thickness (●) and mean pore width (◆) for n-InP electrodes after an LPS at 2.5 mV s^{-1} from 0 to 0.825 V, 0.675 V, and 0.7 V in 2, 3, and 5 mol dm^{-3} KOH, respectively.
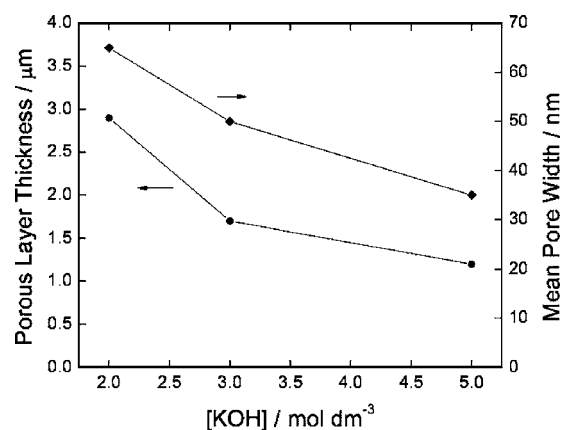

Figure 13. Plots of the porous-layer thickness (●) and mean pore width (◆) for n-InP electrodes after constant-potential anodization for 150 s at 0.75 V in 2, 3, and 5 mol dm^{-3} KOH, respectively.

thickness and a corresponding value of $\sim 10^8$ V m^{-1} for the electric field at the surface at an applied potential of 0.4 V (i.e., where the current increases significantly in Fig. 1a). Further evidence that the anodic process involves holes supplied by a breakdown mechanism of the depletion layer is provided by a comparison of the current-voltage curves for standard ($\sim 3 \times 10^{18}$ cm^{-3}) and higher-doped ($\sim 6 \times 10^{18}$ cm^{-3}) n-InP electrodes (Fig.15). The anodic peak occurs at a lower potential value for the higher-doped InP as a result of the thinner depletion layer (~ 25 nm).

TEM has provided strong evidence that the nanoporous layer forms by the penetration into the surface of localized pits from which the pore propagation is subsequently controlled. For pitting of the surface to occur, a mechanism that limits current flow across the semiconductor-electrolyte interface is necessary to establish the conditions for localized preferential etching.[27] Current limitation could occur due either to the absence of available holes at the surface (i.e., the electric field not being high enough for breakdown of the depletion layer) or to the formation of a passivating oxide film on the surface. Breakdown of the depletion layer at defect sites occurs at lower potentials,[30,35,36] and enhanced etching will occur at these sites resulting in pitting.[17] A similar effect may occur due to breakdown of an otherwise stable oxide film on the surface. Whether pit initiation stems from a breakdown mechanism within the semicon-
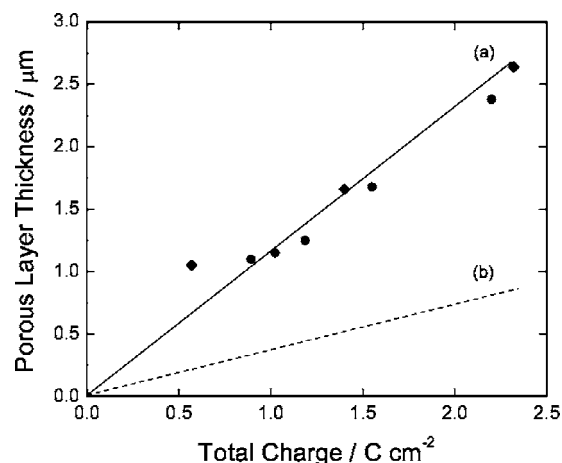

Figure 14. (a) Plot of porous-layer thickness for InP samples anodized at constant potential (●) and after an LPS (◆) as a function of the charge passed. (b) The theoretical thickness of a dense layer corresponding to the amount of InP oxidized.
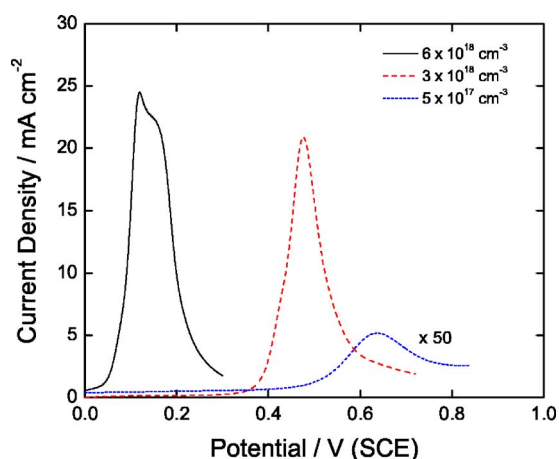
Figure 15. (Color online) LSVs of n-InP electrodes with three different carrier concentrations in 5 mol dm^{-1} KOH at 2.5 mV s^{-1}. The current scale is magnified by 50 for the lower doped sample.

ductor or from breakdown of a surface film, the resulting effect is the same: pitting of the substrate occurs. Once a pit is formed, the electric field is greatly enhanced due to the small radius of curvature at the base of any given pit. Preferential hole generation thus occurs in the vicinity of the pit tip, leading to an enhanced etch rate and consequent pore growth. The electrolyte within the porous structure is connected to the bulk electrolyte by the channels through the dense near-surface layer enabling ionic current flow and mass transfer so that etching then proceeds at pore tips.
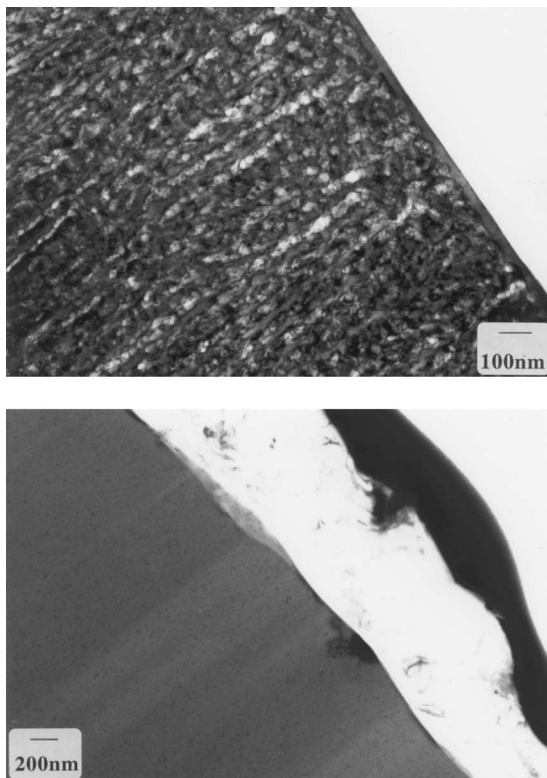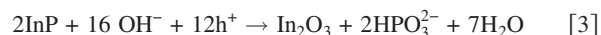

Figure 16. (a) Cross-sectional bright-field TEM micrographs of (a) higher-doped ($\sim 6 \times 10^{18}$ cm^{-3}) InP electrode following an LPS at 2.5 mV s^{-1} in 5 mol dm^{-3} KOH from 0 to 0.3 V (SCE) and (b) lower-doped ($\sim 5 \times 10^{17}$ cm^{-3}) InP following an LPS at 2.5 mV s^{-1} in 5 mol dm^{-3} KOH from 0 to 0.85 V (SCE).

The existence of a dense near-surface layer appears to be related to the depletion layer. The near-surface layer thickness for the more highly doped InP ($\sim 6 \times 10^{18}$ cm^{-3}) is ~ 25 nm (Fig. 16a) by comparison with ~ 40 nm for the standard InP electrode (Fig. 2a). The estimated thickness of the depletion layer is ~ 20 nm for the more highly doped InP as compared with ~ 30 nm for standard samples, indicating that the thickness of the near-surface layer scales with that of the depletion layer. In both cases, the interpore distance of the InP is similar to the near-surface InP layer, suggesting that this dimension is also related to the depletion layer. Such a relationship to the thickness of the near-surface and interpore InP is reasonable if the etching process is controlled by holes supplied by breakdown of the depletion layer.

The detailed electrochemistry of nanoporous InP formation requires further investigation, but it is speculated that etching occurs directly by a process such as

$$2\text{InP} + 22 \text{ OH}^- + 16\text{h}^+ \rightarrow \text{In}_2\text{O}_3 + 2\text{PO}_4^{3-} + 11\text{H}_2\text{O} \quad [2]$$

or

$$2\text{InP} + 16 \text{ OH}^- + 12\text{h}^+ \rightarrow \text{In}_2\text{O}_3 + 2\text{HPO}_3^{2-} + 7\text{H}_2\text{O} \quad [3]$$

where h$^+$ denotes a hole, leading to the formation of In$_2$O$_3$ and oxo-anions of phosphorus in solution. The formation of PO$_4^{3-}$ (a P$^\text{V}$ oxo-anion) corresponds to an eight-electron (per InP) process, while the formation of a P$^\text{III}$ oxo-anion such as HPO$_3^{2-}$ corresponds to a six-electron process.

Conclusions

Anodization of highly doped (10^{18} cm^{-3}) n-InP in 2–5 mol dm^{-3} KOH under potentiostatic or potentiodynamic conditions resulted in the formation of a nanoporous subsurface region beneath a thin (typically ~ 40 nm) dense near-surface layer. LSVs showed a pronounced anodic peak, typically at 0.48 V for a 2.5 mV s^{-1} scan in 5 mol dm^{-3} KOH, corresponding to the formation of the porous region. Current-time curves at constant potentials in the range 0.5–0.75 V similarly showed current peaks. However, no porous regions were formed during anodization in 1 mol dm^{-3} KOH.

Nanoporous layers formed under various conditions were, examined by cross-sectional TEM. The porous region was typically 1-3 μm in thickness, depending on the formation conditions: the thickness decreased with increasing KOH concentration. Pore widths were typically in the range 25–75 nm and decreased with increasing KOH concentration. The porosity was approximately 35%.

The thickness of the near-surface layer and the interpore spacing both decreased with increasing carrier concentration and appeared to scale with the estimated thickness of the electron depletion layer at the semiconductor surface at the potential where etching occurred. The potential of the anodic current peak decreased with increasing carrier concentration, consistent with electric-field-induced breakdown of the depletion layer.

TEM evidence was obtained that the nanoporous layer structure is formed by penetration of surface pits to form channels through the dense near-surface layer at particular points with pore propagation within the InP originating at these points. Such channels provide the required connectivity between the bulk electrolyte and porous region, thus enabling etching to proceed at the pore tips. The dense near-surface layer is believed to originate from electron depletion at the semiconductor surface.

References

1. L. T. Canham, *Appl. Phys. Lett.*, **57**, 1046 (1990).
2. V. Lehman and H. Föll, *J. Electrochem. Soc.*, **137**, 653 (1990).
3. H. Föll, *Appl. Phys. A*, **53**, 8 (1991).
4. T. Holeç, T. Chvojka, I. Jelínek, J. Jindrich, I. Nemec, I. Pelant, J. Valenta, and J. Dian, *Mater. Sci. Eng., C*, **19**, 251 (2002).
5. R. J. Martín-Palma, J. M. Martínez-Duart, L. Li, and R. A. Levy, *Mater. Sci. Eng., C*, **19**, 359 (2002).
6. A. Matoussi, T. Boufaden, A. Missaoui, S. Guermazi, B. Bessaïs, Y. Mlik, and B. El Jani, *Microelectron. J.*, **32**, 995 (2001).
7. A. Jain, S. Rogojevic, S. Ponoth, N. Agarwal, I. Matthew, W. N. Gill, P. Persans, M. Tomozawa, J. L. Plawsky, and E. Simonyi, *Thin Solid Films*, **398**, 513 (2001).
8. N. E. Chayen, E. Saridakis, R. El-Bahar, and Y. Nemirovsky, *J. Mol. Biol.*, **312**, 591 (2001).
9. S. Langa, J. Carstensen, M. Christophersen, H. Föll, and I. M. Tiginyanu, *Appl. Phys. Lett.*, **78**, 1074 (2001).
10. G. Oskam, A. Natarajan, P. C. Searson, and F. M. Ross, *Appl. Surf. Sci.*, **119**, 160 (1997).
11. M. M. Faktor, D. G. Fiddyment, and M. R. Taylor, *J. Electrochem. Soc.*, **122**, 1566 (1975).
12. F. M. Ross, G. Oskam, P. C. Searson, J. M. Macaulay, and J. A. Liddle, *Philos. Mag. A*, **75**, 2 (1997).
13. C. O'Dwyer, D. N. Buckley, V. J. Cunnane, D. Sutton, M. Serantoni, and S. B. Newcomb, in *Proceedings of the State-of-the-Art Program on Compound Semiconductors XXXVII*, P. C. Chang, W. K. Chan, D. N. Buckley, and A. G. Baca, Editors, PV 2002-14, p. 259, The Electrochemical Society, Proceedings Series, Pennington, NJ (2002).
14. S. Langa, J. Carstensen, I. M. Tiginyanu, M. Christophersen, and H. Föll, *Electrochem. Solid-State Lett.*, **4**, G50 (2001).
15. S. Langa, J. Carstensen, I. M. Tiginyanu, M. Christophersen, and H. Föll, *Electrochem. Solid-State Lett.*, **3**, 514 (2000).
16. E. Harvey, C. O'Dwyer, T. Melly, D. N. Buckley, V. J. Cunnane, D. Sutton, S. B. Newcomb, and S. N. G. Chu, in *Proceedings of the State-of-the-Art Program on Compound Semiconductors XXXV*, P. C. Chang, S. N. G. Chu, and D. N. Buckley, Editors, PV 2001-2, p. 87, The Electrochemical Society, Proceedings Series, Pennington, NJ (2001).
17. P. Schmuki, J. Fraser, C. M. Vitus, M. J. Graham, and H. S. Isaacs, *J. Electrochem. Soc.*, **143**, 3316 (1996).
18. P. Schmuki, D. J. Lockwood, J. Fraser, M. J. Graham, and H. S. Isaacs, *Mater. Res. Soc. Symp. Proc.*, **431**, 439 (1996).
19. M. Christopherson, J. Carstensen, A. Feuerhake, and H. Föll, *Mater. Sci. Eng., B*, **69**, 70,194 (2000).
20. S. Rönnebeck, J. Carstensen, S. Ottow, and H. Föll, *Electrochem. Solid-State Lett.*, **2**, 126 (1999).
21. P. Schmuki, L. E. Erickson, D. J. Lockwood, J. W. Fraser, G. Champion, and H. J. Labbé, *Appl. Phys. Lett.*, **72**, 1039 (1998).
22. B. H. Erne, D. Vanmaekelbergh, and J. J. Kelly, *J. Electrochem. Soc.*, **143**, 305 (1996).
23. J. Carstensen, M. Christophersen, and H. Föll, *Mater. Sci. Eng., B*, **69-70**, 23 (2000).
24. S. Langa, J. Carstensen, I. M. Tiginyanu, M. Christophersen, and H. Föll, *Electrochem. Solid-State Lett.*, **5**, C14 (2002).
25. S. Langa, J. Carstensen, M. Christophersen, K. Steen, S. Frey, I. M. Tiginyanu, and H. Föll, *J. Electrochem. Soc.*, **152**, C525 (2005).
26. S. M. Sze, *Physics of Semiconductor Devices*, 2nd ed., John Wiley & Sons, New York (1981).
27. I. E. Vermier, H. H. Goosens, F. Vanden Kerchove, and W. B. Gomes, *J. Electrochem. Soc.*, **139**, 1389 (1992).
28. L. A. Giannuzzi and F. A. Stevie, *Micron*, **30**, 197 (1999).
29. R. Lynch, C. O'Dwyer, I. Clancy, D. Corcoran, and D. N. Buckley, in *Proceedings of the State-of-the-Art Program on Compound Semiconductors XLI*, A. G. Baca, W. K. Chan, K. Shiojima, and R. F. Kopf, Editors, PV 2004-6, p. 85, The Electrochemical Society, Proceedings Series, Pennington, NJ (2004).
30. C. O'Dwyer, Ph.D. Thesis, University of Limerick (2003).
31. C. O'Dwyer, D. N. Buckley, D. Sutton, M. Serantoni, and S. B. Newcomb, *J. Electrochem. Soc.*, In press.
32. G. S. Popkirov and R. N. Schindler, *Electrochim. Acta*, **39**, 2025 (1994).
33. P. Jaguiro, S. La Monica, S. Lazarouk, and A. Ferrari, in *Proceedings of Pits and Pores: Formation, Properties and Significance for Advanced Luminescent Materials*, P. Schmuki, D. J. Lockwood, H. Isaacs, and A. Bsiesy, Editors, PV 1997-7, p. 358, The Electrochemical Society, Proceedings Series, Pennington, NJ (1997).
34. *CRC Handbook of Chemistry and Physics*, 81st ed., D. R. Lide, Editor, CRC Press, New York (2000).
35. A. Yammamoto and S. Yano, *J. Electrochem. Soc.*, **122**, 260 (1975).
36. M. J. Theunissen, *J. Electrochem. Soc.*, **119**, 351 (1972).